PHILOSOPHICAL MAGAZINE A, 1998, VOL. 77, NO. 3, 593–619

Structure and phason energetics of Al–Co decagonal phases

By ERIC COCKAYNE

Department of Applied Physics, Yale University, PO Box 208284, New Haven, Connecticut 06520-8284, USA

and MIKE WIDOM

Department of Physics, Carnegie-Mellon University, Pittsburgh, Pennsylvania 15217, USA

[*Received 9 April 1997 and accepted in revised form 30 June 1997*]

ABSTRACT

We develop a model for Al–Co decagonal quasicrystals and approximants. Our model defines a large number of potential atomic positions. These sites are populated by two atomic species that interact with each other through electronic-structure-based pair potentials. Monte Carlo simulation of the model produces realistic atomic configurations for Al–Co alloys in the temperature and composition ranges where a metastable decagonal quasicrystal exists. The resulting structures generally consist of packings of space by pentagonal bipyramid clusters. Projections of the centres of these clusters form tilings of hexagons, boats and stars. We identify atomic displacements associated with phason fluctuations. We note a distinction between 'simple' phason *hops* involving predominantly Al atom motion and 'collective' phason *flips* that transport the Co atoms.

§ 1. INTRODUCTION

A fundamental question in the science of quasicrystals is: where are the atoms (Bak 1986a)? Experiments provide partial answers but often cannot resolve the precise position or chemical identity of a small subset of the atoms. Theory can assist experiment. As in ordinary crystallography (Stout and Jensen 1989), total energies for plausible configurations consistent with experimental data can be calculated, and the more favourable structures identified. In addition to improving our knowledge of where the atoms are, we receive a bonus of understanding *why* they choose particular positions. Further, we can identify important structural changes and associated energetics. A topic of lively debate in quasicrystal science is the distinction between entropy and energy stabilization of the quasicrystalline state (Widom 1990, Henley 1991, Ingersent 1991, Socolar 1991). Accurate structural models and total energy calculations can help to resolve this debate. The modelling presented in this paper is unbiased with regard to the mechanism of quasicrystal stabilization.

Early theories of quasicrystals focused on tilings of space without explicit reference to the relationship between individual tiles and real atoms. Cluster models propose reasonable local atomic structures but may leave a small amount of empty space around the clusters, or else suffer from unreasonably short interatomic distances. Similar difficulties plague 'atomic surface' (Bak 1986b) descriptions of

quasicrystal structure. These difficulties led to a proliferation of nearly identical proposed structures differing from one another mainly in the placement or chemical identity of a small number of atoms. We feel that is important to compare possible structures with each other systematically, discriminating on the basis of total energy (Cockayne *et al.* 1993, Phillips and Widom 1993) for zero-temperature stability, and free energy at finite temperatures.

Recently, *ab initio* electronic structure calculations have been used in the case of Al–Pd–Mn to find the most stable large decagonal approximants (Krajčí *et al.* 1997). To investigate structures as complex as quasicrystals and their approximants at thermal equilibrium, however, it is necessary to be able to evaluate energies for large number of configurations rapidly. First-principles methods are not practical at present; therefore effective interatomic potentials are required.

All known *stable* icosahedral (i-) and decagonal (d-) quasicrystals (i-(Al–Cu–Fe) (Tsai *et al.* 1987), d-(Al–Cu–Co), d-(Al–Ni–Co) (Tsai *et al.* 1989), i-(Al–Pd–Mn) (Tsai *et al.* 1990), etc.) are at least ternary compounds. To date, no effective interatomic potentials are known for any stable quasicrystal-forming systems, so attention must be focused on binary alloys. Electronic-structure-based pair potentials exist for binary alloys of Al with Co (Phillips *et al.* 1994) and Mn (Zou and Carlsson 1993a,b). The binary Al–Co alloy is a good system to study via pair potentials, because it contains a metastable quasicrystalline phase. Related stable crystal phases possess local structures with fivefold symmetry. Al and Co are also constituents of stable d-(Al–Cu–Co) and d-(Al–Ni–Co). This paper describes in detail our investigation of Al–Co alloys related to decagonal quasicrystals (Widom and Cockayne 1995, 1996).

Several stable and metastable complex phases occupy a small composition interval in the binary $Al_{1-x}Co_x$ system for $0{\cdot}23 \leqslant x \leqslant 0{\cdot}29$ (Grushko *et al.* 1995). Most of these phases, including a decagonal phase (d-Al–Co)), share an 8 Å stacking periodicity in the z direction and possess similar structural units separated in the plane by 6·5 Å. These structural units form tilings of hexagons in the solved structures of monoclinic $Al_{13}Co_4$ (Hudd and Taylor 1962) and orthorhombic Al_3Co (Grin *et al.* 1994, Li *et al.* 1994, Widom *et al.* 1995) and appear to form tilings of hexagons, boats (crowns) and stars in high-resolution electron microscopy images of larger approximant phases (Ma and Kuo 1995). We shall sometimes refer to this family of related structures under the name 'Al_3Co'. The fact that tiles shaped like hexagons, boats and stars comprise the Al_3Co structures suggests that the same tiles also comprise the decagonal phase. We call this model the 'hexagon–boat–star (HBS) tiling model' (Li 1995) for d-(Al–Co). The simplest quasiperiodic HBS tiling is given by a subset of the vertices of the two-dimensional (2D) Penrose tiling and is an example of a 'two-level tiling' (Tang and Jarič 1990, Li and Kuo 1991, Henley 1991, 1993) (fig. 1 (*a*)). Many other HBS tilings are also possible (fig. 1 (*b*)). A slight variation on the HBS tiling model, where a fourth tile shaped like a decagon is allowed (Li 1995), seems to describe decagonal phases such as d-(Al–Pd–Mn) (Li and Dubois 1994). We call this the 'HBSD' model.

The solved low-temperature Al_3Co structures alternate flat (F) and puckered (P) layers of atoms separated by approximately 2 Å and have a periodicity of four layers in the z direction. The stacking sequence is FPF′P′, where F′ is a variant of F, and P′ is P mirrored in a horizontal plane. The only known exception, $Al_{11}Co_4$ (Li *et al.* 1995), is stable only at high temperatures. It alternates layers similar to the F and P types with a net 4 Å periodicity and is closely related to the 8 Å structures. Structural

Fig. 1

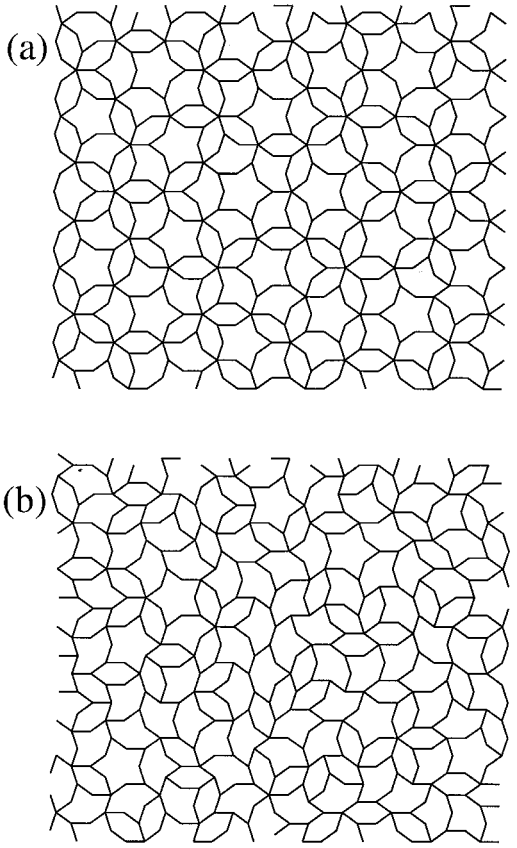

(*a*) Two-level HBS tiling formed by removing a subset of vertices from the Penrose rhombus tiling. (*b*) Random HBS tiling.

units separated horizontally by 6·5 Å consist of $Al_{16}Co_7$ pentagonal bipyramids (PBs) (fig. 2). The equator of the PB features a pentagon of Co atoms in a flat layer with edge length 4·7 Å centred by an Al atom. Co atoms in adjacent puckered layers lie on the (pseudo)pentagonal axis of the PB and are forced away from this central Al, causing puckering of those layers. The PB occupies three layers along the stacking axis. Two PBs separated by c = 8 Å along *z* are joined by a fourth 'junction' layer consisting of a highly distorted pentagon of Al (including frequent vacancies) in a flat layer. Flat layers F and F′ differ by interchanging PB equators with PB junctions. Figure 3 shows the recently solved structure (Grin *et al.* 1994) of orthorhombic Al_3Co. PB equators and flat-layer junctions are visible in fig. 3(*a*), while the PB caps fill fig. 3(*b*).

Because two flat layers occur per 8 Å along the stacking axis, there are two choices of level on which to centre the PB. When centred on the flat layer F we label the PB '+'. The Co in layer P, just above F, is displaced upwards to accommodate the centring Al. When centred on the flat layer F′ we label the PB '−'. The Co in P just below F′ is then displaced downwards. Vertical displacement of Co

Fig. 2

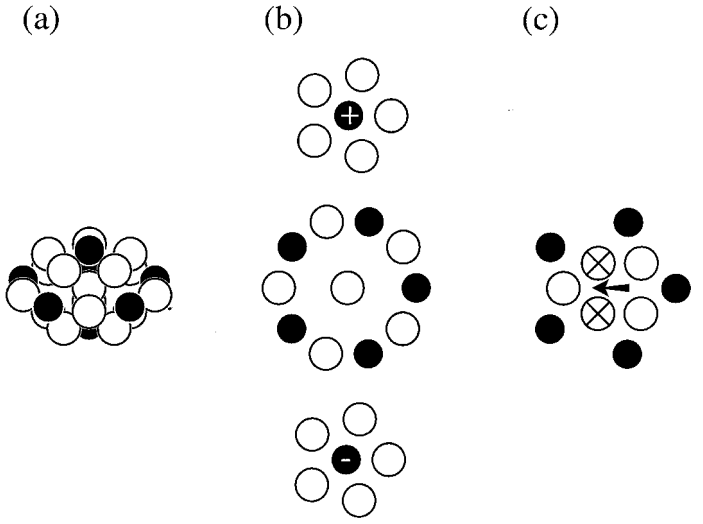

(*a*) PB cluster containing 16 Al and seven Co atoms. (*b*) Exploded view showing equator and caps. In both simulated and observed structures, some equator Al atoms are displaced to the midpoints of their Co neighbours. (*c*) Flat-layer junction. All Al sites have partial occupancy. The sites labelled × also have partial Co occupancy. The long axis of the distorted pentagon defines an orientation, indicated by the arrow.

atoms in puckered layers relates to the centring of PBs in layers F or F′. Because our description is Ising like (i.e. a Z_2 symmetry), we use the Ising spins to describe the centring of the PBs or the 'puckering pattern'. Figure 4 shows the puckering patterns observed in monoclinic $Al_{13}Co_4$ and orthorhombic Al_3Co.

Combining the HBS tiling model with the PB structure described above suggests that the 8 Å decagonal phase consists of PBs on the vertices of a HBS tiling. We call this model the 'PB-HBS tiling model' for 8 Å decagonal phases. The model 'PB8' proposed by Henley (1993) was a PB–HBS tiling model. Significant structural rearrangements are easily described within the context of the PB–HBS tiling model. A transformation, which effectively shifts the centres of the PBs in a single column by 4 Å along the column, changes the sign of the PB. We call this transformation a 'puckering flip'. A second transformation is the minimal transformation that changes one HBS tiling into another. We call this transformation a 'phason flip'. An alternate name for this transformation would be 'tiling flip, and we use the two names synonymously. In a phason flip, the PBs in one column effectively shift by 2·5 Å and rotate 180°.

In this paper, we explore the thermodynamics, equilibrium structures and energetics of 8 Å periodicity Al–Co alloys with a finite-temperature Monte Carlo method. Among our results, we found the following

(1) Favoured atomic configurations are well described within the PB–HBS model.
(2) The average structure of a 508-atom approximant is found and presented as atomic surface maps. Co atoms mainly occupy atomic surface interiors.

Fig. 3

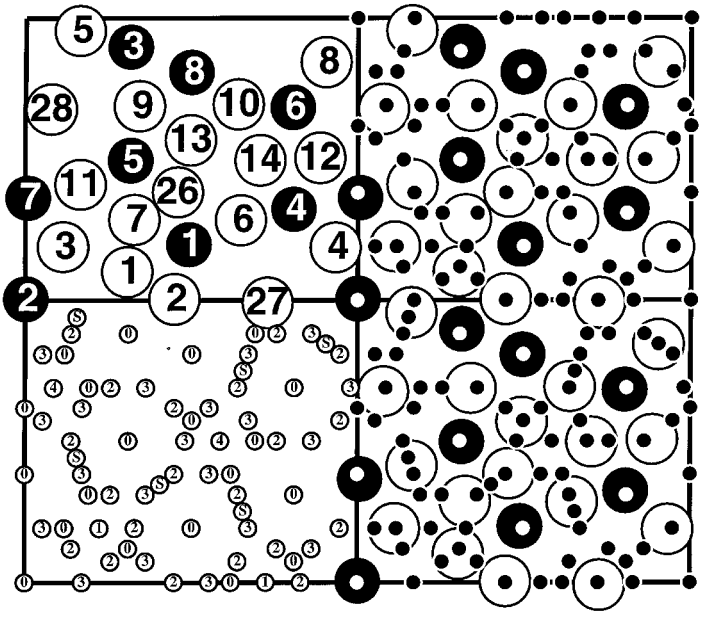

(*a*)

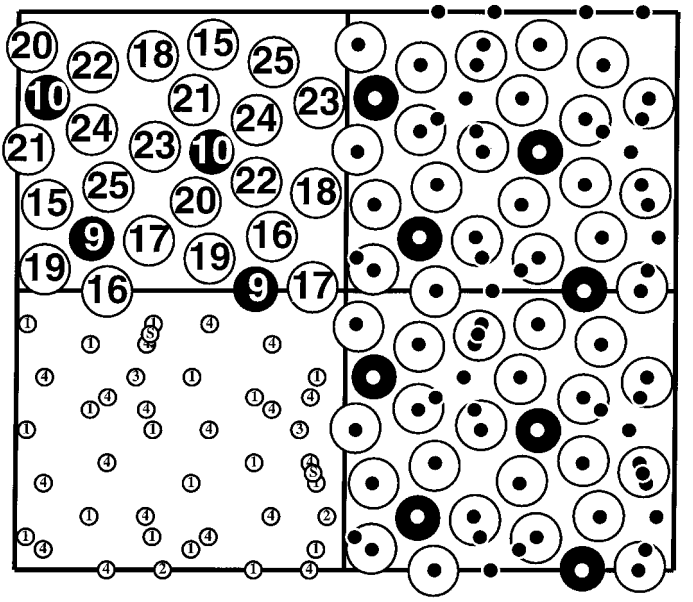

(*b*)

Experimental and ideal atomic sites for the 2/3 approximant in (*a*) a flat layer F and (*b*) a puckered layer P. Clockwise from lower left: ideal and averaged sites labelled with atomic surface numbers; experimental structure (atoms labelled as in the structure refinement of Grin *et al.* (1994)); ideal and experimental superimposed; same with averaged sites added.

Fig. 4

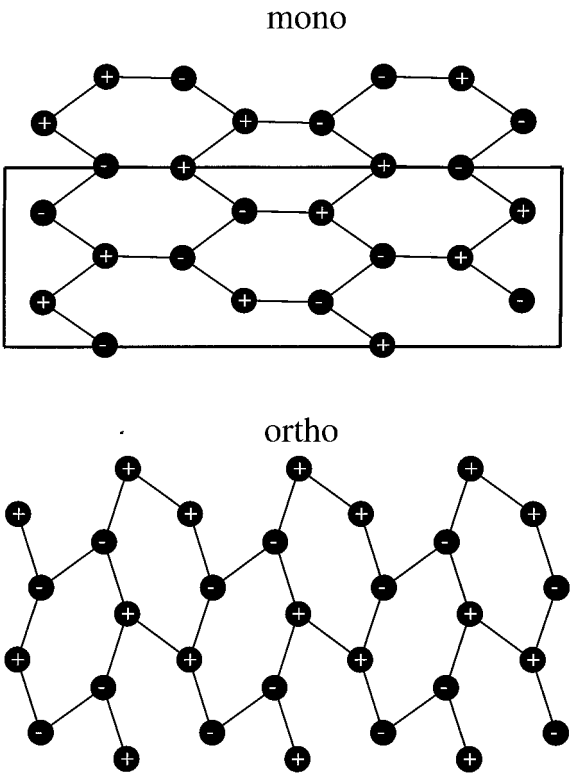

Tiling and puckering patterns observed in (*a*) monoclinic $Al_{13}Co_4$ and (*b*) orthorhombic Al_3Co. The pseudocentred orthorhombic supercell of the monoclinic phase is highlighted.

(3) Phason disorder similar to partial occupancy in quasicrystal approximants (Hudd and Taylor 1962, Mahne and Steurer 1996) is prevalent at Al sites near atomic surface edges.
(4) Individual atomic phason hops (Frenkel *et al.* 1986) and collective atomic motions resulting in puckering flips or phason flips turn out to cost little energy.

The following section presents model atomic surfaces chosen to be consistent with known Al–Co crystalline approximant phases, and to generalize those structures to the quasicrystal. In § 3 our Monte Carlo simulation method and the pair potentials used for total energy calculations are explained. In § 4 our main results on structure (§ 4.1) and energetics § 4.2 are described. Finally, in § 5, our key results are summarized, and improved methods for future studies are discussed.

§ 2. Atomic surfaces

Quasicrystalline structures can be succinctly described in terms of atomic surfaces (Bak 1986b). Although the shapes of atomic surfaces for a quasicrystal are not necessarily *simple* (Gähler 1988, Cockayne 1995), diffraction experiments on

decagonal quasicrystals (Steurer and Kuo 1990, Steurer 1991, Steurer *et al.* 1993, 1994) show that the vast majority of atoms belong to a set of distinct atomic surfaces, and that these atomic surfaces are relatively flat. They are strongly localized in 'parallel space' while being quite extended in 'perpendicular space'. Since the precise shapes of the atomic surfaces for the d-(Al–Co) structure are unknown, we include in this work all the sites that belong to a set of oversized atomic surfaces. The number of sites included is therefore much greater than the number of atoms. Atomic surface sizes and shapes are deliberately chosen to include any likely low-energy structure as well as the dominant fluctuations about these structures.

In the following we use the cut method, beginning with a five-dimensional (5D) lattice. The three-dimensional (3D) physical (parallel) and 2D perpendicular space components of the 5D basis vectors used here are

$$\begin{aligned}\mathbf{e}_i &= \left[(\mathbf{e}_i^{\parallel}),(\mathbf{e}_i^{\perp})\right] \\ &\equiv \begin{cases} \left[a_0\left(\cos\left(\frac{2\pi i}{5}\right),\sin\left(\frac{2\pi i}{5}\right),0\right), a_0\left(\cos\left(\frac{6\pi i}{5}\right),\sin\left(\frac{6\pi i}{5}\right)\right)\right], & i<5, \\ (0,0,c,0,0), & i=5, \end{cases}\end{aligned} \tag{1}$$

where a_0 (the quasilattice constant) and c are lattice parameters to be determined by experiment. We use $a_0 = 1{\cdot}529$ Å and $c = 8{\cdot}120$ Å for our calculations. Most atomic surfaces are centred on 5D sites of the form (n_1, n_2, n_3, n_4, z), that is the first four coordinates are integer. In this case, we define the level υ of the atomic surface to be

$$\upsilon = \left(\sum_{j=1}^{4} n_j\right) \bmod 5. \tag{2}$$

Since the atomic surfaces are distinguished by coordinate υ, the actual periodicity of the 5D structure is the superlattice of the lattice generated by eqn. (1) which leaves υ invariant. An atom in the quasicrystal located at position $\mathbf{r}$ has $(\mathbf{r}^{\parallel}, \mathbf{r}^{\perp}) = (\mathbf{r}, 0)$ and is associated with a nearby 'ideal site':

$$(\mathbf{r},0) = (\mathbf{r}_{\text{ideal}},0) + (\Delta\mathbf{r}^{\parallel},0), \tag{3}$$

$$(\mathbf{r}_{\text{ideal}},0) = \sum_{j=1}^{4} n_j(\mathbf{e}_j^{\parallel},\mathbf{e}_j^{\perp}) + z(\mathbf{e}_5^{\parallel},\mathbf{e}_5^{\perp}) + (0,\Delta\mathbf{r}^{\perp}). \tag{4}$$

For an approximant, eqns. (3) and (4) still hold, except that the form of the $\mathbf{e}_i^{\perp}$ in eqn. (1) must be altered appropriately (Edagawa *et al.* 1991, Fettweis *et al.* 1994).

For a given atom, the decomposition into $\{n_j\}$ is not unique, but in the solved Al_3Co approximants, nearly all the atoms have a unique solution to eqns. (3) and (4) such that $|\Delta\mathbf{r}^{\parallel}| < 0{\cdot}4$ Å and $|\Delta\mathbf{r}^{\perp}| < a_0$. For such atoms, we call $\mathbf{r}_{\text{ideal}}$ the *ideal site* for the atom. Inserting the corresponding values for n_j in eqn. (4) into eqn. (2), we find the value of υ associated with the ideal site and with the atom itself. Two atoms whose ideal sites are separated by $\tau a_0 = 2{\cdot}5$ Å (a typical atomic near-neighbour distance) differ in υ by 2 (modulo 5). Centres of PBs, ideally separated by $\tau^3 a_0 = 6{\cdot}5$ Å, also differ in υ by 2 (modulo 5).

From structures of solved approximants, we find appropriate atomic surface locations. We set the ideal sites for PB centres at levels 1 and 4, in agreement with the notation of Steurer and Kuo (1990) and Steurer *et al.* (1993). Most remaining

Table 1. List of important distances in our model. For Al–Co, we use quasilattice parameter $a_0 = 1{\cdot}529$ Å, periodicity along decagonal axis $c = 8{\cdot}120$ Å and puckering parameter $p = 0{\cdot}260$ Å.

Total distance (Å)	In-plane distance	Vertical distance	Total distance (Å)	In-plane distance	Vertical distance
0·260	0	p	2·353	$\tau \cos(\pi/10)\, a_0$	0
0·520	0	$2p$	2·474	τa_0	0
0·539	$\tau^{-1} a_0/2$	p	2·908	$2 \cos(\pi/10)\, a_0$	0
0·765	$a_0/2$	0	4·706	$2\tau \cos(\pi/10)\, a_0$	0
0·945	$\tau^{-1} a_0$	0	5·532	$5^{1/2}\tau a_0$	0
1·529	a_0	0	6·477	$\tau^3 a_0$	0
2·290	0	$c/4 + p$	7·614	$2\tau^2 \cos(\pi/10)\, a_0$	0
2·339	a_0	$c/4 - p$	8·120	0	c

atoms in the flat layers occupy levels 0, 2 and 3. The puckered layers are simpler; nearly all the sites occupy levels 1 and 4 (see fig. 3). Although the z coordinates of the puckered-layer atoms take a range of values, we make the simplifying approximation that all such atoms, except for certain 'unpuckered' atoms described in the following paragraph, are located at exactly $(0, c/2) \pm p$, where p is a 'puckering parameter' for Al–Co. From the solved $Al_{13}Co_4$ structure, we averaged the z coordinates for the puckered-layer atoms appropriately to obtain $p \approx 0{\cdot}26$ Å. For convenience, we compiled a list of useful intersite distances in table 1.

Three types of atomic site that occur in the orthorhombic Al_3Co approximant are difficult to represent in terms of flat atomic surfaces. Using the notation of Grin *et al.* (1994), these are sites of type Al(7)–Al(26), Al(8) and Al(18) (see fig. 3). The latter two lie at sites of approximate inversion symmetry: Al(8) in the flat layer at the midpoint between two edge-sharing PBs; Al(18) in the puckered layer where two empty pentagons of Al meet tip to tip at the centre of a long hexagon of PBs. In each of these two cases, ideal sites with integer coordinates lie symmetrically placed nearby. For the Al(8) sites, atomic surface 2 and 3 sites lie 0·76 Å away. For the Al(18) sites, atomic surface 1 and 4 sites lie 0·54 Å away, 0·47 Å in plane and 0·26 Å vertically. The vertical puckerings occur in opposite directions; so the averaged site is 'unpuckered', as is nearly the case experimentally. We define the appropriate averages of the nearby ideal sites as extra 'special' sites, shown in fig. 3.

The remaining difficult sites, the Al(7)–Al(26) pair, lie in the flat layer near the midpoint of a PB edge shared by two clusters and are asymmetrically displaced 1·34 Å and 0·90 Å respectively, toward the centres of the two clusters (Grin *et al.* 1994). A pair of atomic surface 2 and 3 sites exist in similar positions, but with smaller and symmetric 0·76 Å displacements from the edge (see fig. 3). The Al(7) and Al(26) sites lie 0·58 Å and 0·14 Å respectively, away from from these ideal sites. We rely on the existing ideal sites to approximate the Al(7)–Al(26) class of sites. The ideal sites are 1·53 Å apart while the experimental sites are 2·24 Å apart. In either case, the sites are so close together that it would be very costly energetically for both sites to be simultaneously occupied by Al.

In all cases except the Al(7)–Al(26) pair, the displacement of experimental sites from ideal is less than 0·38 Å. To visualize the coincidence between ideal and experimental positions, consider spheres of radius 0·38 Å placed around every ideal site. Only 5% of the total volume of space would be filled, but 99% of the experimental

sites would be covered by these spheres. The median deviation of experimentally measured sites from the nearest ideal site is 0·12 Å, a distance smaller than typical displacements due to thermal phonons at room temperature.

We extend the above analysis to find reasonable atomic surface shapes and sizes for larger approximants and the decagonal phase. We exploit the fact that the atomic arrangements observed in the Al–Co approximants are locally two- or three-level packings and the fact that there is a very convenient limit to the range of atomic surface shapes for a good two- or three-level packing: the atomic surfaces for levels υ, $\upsilon + 2$ and $\upsilon - 2$ lie within decagons of radius a, a and τ^{-2}a respectively (Olamy and Kléman 1989, Niizeki 1994). The Al–Co approximants show that levels 0, 2 and 3 dominate in certain regions of the flat planes (see fig. 3). These atomic surfaces are set to be decagons of radius a, while the atomic surfaces for levels 1 and 4 are set to radius τ^{-2}a. In the puckered layers, the occupied sites in the solved structures are exclusively level 1 and level 4 sites (or their averages as described above). We choose decagons of radius a for levels 1 and 4. We also include atomic surfaces of radius τ^{-2}a at levels 2 and 3 to allow for the possibility of three-level packings in these layers.

The difficulty extrapolating from approximants to the quasicrystal is that the quasicrystal itself may contain sites cut from atomic surfaces so small that they are not contained in small approximants. For example, a boat and two hexagons could combine to form a decagon of 20 Å diameter, reducing the number of vertices, as shown in fig. 5. The interior of an asymmetric 20 Å decagon in a PB–HBS tiling could undergo reconstruction to a decagonally symmetric arrangement (Beeli and

Fig. 5

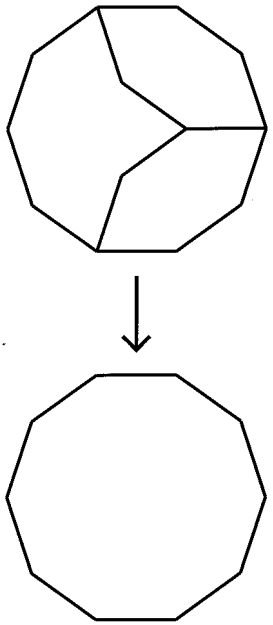

Possible reconstruction of two hexagons and a boat of edge length 6·5 Å into a symmetric decagon of diameter 20 Å.

Table 2. Atomic surfaces included. We used $\epsilon = \tau^{-3}/2 \approx 0{\cdot}118$ in this study. The remaining atomic surfaces differ only in their z coordinate and generated by $z + 0{\cdot}5$ and $-z$. The average electron count in individual atomic surfaces as determined by simulation, showing the absence of certain atomic surfaces.

z	Level(s)	Multiplicity	Radius (units of $a_\perp$)	Average electron count (simulated)
0·25	0	2	$1 + \epsilon$	702
0·25	2, 3	4	$1 + \epsilon$	140
0·25	1, 4	4	$\tau^{-2} + \epsilon$	27
0·25	(Averaged)	10	(See text)	18
0·282	0	4	$\tau^{-3} + \epsilon$	13
0·468	1, 4	8	$1 + \epsilon$	227
0·468	2, 3	8	$\tau^{-2} + \epsilon$	0
0·5	0	2	$\tau^{-3} + \epsilon$	0
0·5	(Averaged)	10	(See text)	21

Horiuchi 1994), turning it into a PB–HBSD tiling. The solved Al–Co approximants are too small to contain the motifs shown in fig. 5 and hence cannot distinguish between a HBS tiling quasicrystal and a HBSD tiling quasicrystal. The centres of reconstructed decagons would be level 0 points and could naturally accommodate a (distorted) pentagonal bipyramid. For maximal local symmetry, these bipyramids would be centred at *unpuckered* positions in the puckered layer and the 'pole' atoms would then be *puckered* positions in the flat layer. These potential sites are associated with the small atomic surfaces of radius $\tau^{-3}a$ included in table 2. We thus allow for the possibility of HBSD tilings in our system. Note how the distinction between HBS and HBSD tilings depends on very small atomic surfaces, that is a very small fraction of the atoms.

With the atomic surface radii described above, the site list allows for a variety of quasiperiodic and approximant structures. Certain phason fluctuations cannot be represented, however, because the final atomic position would be outside this set. To model these fluctuations, which we expect to be important, we make the atomic surfaces oversized. We keep their decagonal shapes, but expand each radius by $\epsilon \equiv \tau^{-3}a/2 \approx 0{\cdot}12a$. The value of ϵ was chosen to allow for what we estimate to be the important fluctuations while keeping the number of sites from being too large. In a 2D, maximally random random-tiling quasicrystal, for large approximants, ϵ should increase logarithmically (Widom *et al.* 1989, Strandburg *et al.* 1989) as the size of the approximant. For 3D icosahedral quasicrystals it should saturate (Tang 1990). The appropriate behaviour for 3D decagonal quasicrystals with equilibrium stacking disorder is still open to investigation (Henley 1991, Burkov 1991a, Jeong and Steinhardt 1993, Shin and Strandburg 1993).

After the atomic surfaces are oversized, we add the special sites with half-integer coordinates. All flat layer positions midway between level 1 and level 4 flat-layer sites separated by 6·5 Å are added to the list, in order to include sites equivalent to Al(8) in Al_3Co. Additionally, sites at $z = \{0, 0{\cdot}5\}$ which project to the centre of a 6·5 Å by 7·6 Å rectangle of level 1 and 4 flat-layer sites are included, in order to include sites equivalent to Al(18) in Al_3Cd (see fig. 3).

Finally, all atomic surfaces are repeated at the additional values of z equal to $-z$, $0{\cdot}5 + z$ and $0{\cdot}5 - z$. Addition of the $-z$ sites allows the atoms in the puckered layers to shift to either of two puckering positions 0·26 Å above or below the middle of

their layer. As a consequence, the periodicity of the list of sites is only 4 Å. However, we note that most models for 4 Å periodic decagonal quasicrystals (Steurer and Kuo 1990, Yamamoto *et al.* 1990, Burkov 1991b, Hiraga *et al.* 1991, Steurer *et al.* 1993, E. Cockayne and M. Widom 1996, unpublished) are incompatible with our atomic surfaces because we impose FP alternation ($P10/mmm$ symmetry), while the 4 Å models alternate equivalent layers ($P10_5/mmc$ symmetry), as implied by diffraction studies (Steurer and Kuo 1990).

§ 3. Monte Carlo approach

We employ Monte Carlo simulation to assign atoms to sites. Over long runs, the simulation generates many possible atomic arrangements, each with a probability proportional to its Boltzmann weight. Our simulation uses the Metropolis *et al.* (1953) method, generating a new configuration based upon the present atomic positions, and moving to the new configuration with a probability related to the change in total energy between configurations while obeying the requirement of detailed balance.

New configurations are generated by one of three moves. We permit a 'small hop' of an atom to a neighbouring site less than 2·5 Å away. We also permit 'long hops' to any other site regardless of how far removed. Finally, we include 'species swaps' in which an arbitrarily chosen Al–Co pair exchange positions. In the steady state, the rate of transitions into a configuration must match the rate of transitions out of the configuration. Detailed balance guarantees that the steady-state probability to be in some configuration is proportional to the Boltzmann factor $\exp(-E/k_BT)$ for the configuration.

Long hops and species swaps easily obey detailed balance using the ordinary Boltzmann factor to accept or reject the move. The small hops are more complicated, however, because some sites have more neighbours than other sites do. Consider a small hop from site i to site j leaving all other atoms fixed. Let P_i and P_j be the Boltzmann factors for the initial and final configurations respectively, and E_i and E_j the energies. The rate to go from i to j is

$$R_{i\to j} = \begin{cases} P_i \omega_i f_{ij} \exp(-(E_j - E_i)/k_B T) & \text{if } E_j > E_i, \\ P_i \omega_i f_{ij} & \text{otherwise,} \end{cases} \tag{5}$$

where ω_i is the rate at which we attempt moves out of site i when it is occupied and f_{ij} is the fraction of attempted moves out of site i that go to site j. Let Z_i be the number of sites within the small hop size of site i, so that $f_{ij} = 1/Z_i$. Detailed balance requires equality of rates $R_{i\to j} = R_{j\to i}$, or

$$\frac{\omega_j Z_i}{\omega_i Z_j} = \frac{P_i}{P_j} \exp(-(E_j - E_i)/k_B T). \tag{6}$$

Inspecting eqn. (6) we note that the right-hand side equals unity at thermal equilibrium. In order for our simulation to produce this equilibrium distribution we must choose the rate ω_i of attempted transitions out of each site i in proportion to the number Z_i of sites within the small hop length of the site i.

Provided that the list of possible sites is not too large, one may speed the simulation by pre-calculating atomic interaction energies. First form an array recording values of the interaction energy (including images under periodic boundary

conditions) between an atom of type α at site i and an atom of type β at site j for all pairs of sites i and j and species α and β. Then, to calculate the potential energy of a given atom at site i, just sum the values of this array over each occupied site j. The savings in simulation time is considerable, with a single evaluation of potential energy for our 508 atom system going about 50 times faster than is possible without using pre-calculated values. The disadvantage to this approach is the need to store large arrays in active memory.

Simulation efficiency is important because we need to reach from 10^5–10^6 Monte Carlo steps per atom. Such long runs are needed because of two peculiarities of our calculation.

(1) Acceptance rates are low, typically 0·0026 for small atomic hops at T = 1000 K; so we must attempt large numbers of moves significantly change the configuration.
(2) Average energy differences between configurations are small compared with random thermal fluctuations.

Quasicrystals possess a mode of elastic deformation, known as a phason mode, not found in ordinary crystals. One can conveniently distinguish phason modes from ordinary elastic phonon modes by representing the quasicrystal as a superposition of incommensurate density waves (Lubensky 1988), each with its own phase. Varying the relative phases of the waves with respect to each other creates zero energy 'Goldstone modes' of the quasicrystal. Certain combinations of phase changes (those that transform as vectors under rotation (Lubensky 1988)) generate continuous translations of the structure and correspond, at finite wavelengths, to phonon modes. The orthogonal subspace of phase changes generates phason modes. Whereas phonon modes impart continuous atomic displacements to each atom, phason modes are believed to create discrete atomic hops (Frenkel *et al.* 1986) between nearby ideal sites. It is common to refer to such localized atomic hops as phasons, without regard to spatial correlations among hopping atoms. In the atomic surface description of a quasicrystal, an atom on a site near the edge of an atomic surface can hop to a nearly equivalent site near a different atomic surface edge. Because the two sites are nearly equivalent, the energy difference may be vanishingly small.

Our modelling technique places atoms only at ideal sites generally located at least 0·5 Å apart. Since the expected thermal phonon displacements of about 0·3 Å at T = 1000 K are insufficient to displace atoms from one ideal site to its neighbour, phonons are frozen out in our model. Thus, except for some purely vertical hops that relate to puckering flips, the atomic hops in our simulation are properly described as phason fluctuations. However, we simulate finite unit-cell structures with periodic boundary conditions. These are ordinary (although complex) crystals and should not have phasons as long-wavelength elastic modes. For these crystal structures, the phason hops correspond to a type of internal disorder in which many sites possess fractional occupancy.

Our Monte Carlo method loses the temporal information produced by molecular dynamics, but it retains the thermodynamic equilibrium state. Configurations are sampled with the proper frequency; they just appear in unusual order. In fact, the evolution pathways in the Monte Carlo method can be chosen at our convenience. By explicitly testing discrete atomic hops, atoms may move easily between nearby potential wells without the need to climb the barrier that separates them. Another

move unique to the Monte Carlo method swaps atoms of differing chemical species. In reality this might require the participation of a nearby vacancy or a lattice dilation to give the atoms enough room to move in. Our simulation accomplishes the same task without these complications. We even allow hops and swaps of arbitrarily large distance, further reducing the time necessary for the simulation to equilibrate.

For atomic interactions we use pair potentials previously described by Phillips *et al.* (1994). These pair potentials represent the dominant term in the structural component of cohesive energy. They are derived by calculating the perturbation to an otherwise uniform free-electron density caused by inserting a positively charged ion and then calculating the energy to place a second ion in the electron gas of spatially varying density. The resultant Friedel oscillations in the potentials favour particular interatomic separations consistent with quasicrystalline structures (Widom and Cockayne 1996). Direct d–d interactions between transition-metal (TM) atoms are not included. These may be expected to play a role when TM atoms lie close together (less than about 2·5 Å), but in the actual structures the TM atoms lie 2·9 Å or more apart. The full cohesive energy should include three-body and higher-order interactions. Fortunately, the two-body term alone seems to reproduce adequately the experimentally determined phase diagram in the composition regime of interest up to about 27% Co (Phillips *et al.* 1994).

The pair potentials include a smooth cut-off beyond 10 Å. We employed periodic boundary conditions in our simulations. Typically the simulation cell was just a single unit-cell length along the *a* and *b* axes but was doubled to achieve a length of 16·24 Å along the *c* axis. Thus no atom interacted strongly with periodic images of itself.

§ 4. Results

Using the simulation method outlined in § 3, we acquire data relevant to two important problems: structure and energetics. Most configurations produced in the simulations can be described in terms of cluster packings, allowing us to describe an ideal alloy structure both in real space and in terms of atomic surfaces. By comparing total energies of different configurations we calculate energies of single- and multiple-atom displacements. We identify changes in structure and energy related to phason hops and to puckering and tiling flips.

4.1. *Structure*

We investigated several orthorhombic approximants in the h/k series (Edagawa *et al.* 1991, Fettweis *et al.* 1994). A remarkable number of approximants to different decagonal phases belong to this family (Liao *et al.* 1992). Even the $Al_{13}Co_4$ monoclinic phase can be looked at as a slightly distorted supercell of a 3/2 orthorhombic approximant (see fig. 4). Simulations on periodic approximants allow the atomic structure of small approximants to be compared with known results and the atomic structure of large unsolved approximants to be predicted. The results on the approximants can then be extrapolated to a plausible model for the decagonal quasicrystal phase.

Before any simulation can begin we must decide on an appropriate atomic density and chemical composition. We use a known structure as a guide. The $Al_{13}Co_4$ monoclinic phase (Hudd and Taylor 1962) has 102 sites per unit cell, occupied by 72·8 Al atoms and 24 Co atoms. Assuming that all Co atoms for any h/k approximant belong to PBs and that the PBs lie on an HBS tiling, there are eight

F_{h+k-1} Co per cell, F_i being the ith Fibonacci number (we choose the origin of the Fibonacci series $F_1 = F_2 = 1$). The 'proper' number of Al atoms for the other approximants should be near the closest integer to $72{\cdot}8\tau^{h+k-5}$. This suggests the decagonal phase lies at about $\lim_{n\to\infty}\left[8F_n/(8F_n + 72{\cdot}8\tau^{n-4}\right] \approx 25{\cdot}2\%$ Co, and the approximant phases should converge towards this value. Fortunately, the corresponding electron density is $0{\cdot}1808\,\text{Å}^{-3}$, almost exactly the same as the density in pure Al for which the pair potentials were calculated.

The ideal lattice parameters a and b for an h/k approximant are $a = 5^{1/2}\tau^{h+1}a_0$ and $b = 2\cos(\pi/10)\,\tau^k a_0$. We focus our attention on three particular approximants: the 2/3 approximant, with lattice constants a = 14·48 Å and b = 12·32 Å, with composition $Al_{73}Co_{24}$; the 3/2 approximant with lattice constants a = 23·43 Å and b = 7·61 Å, with the identical composition; the 3/4 approximant with lattice constants a = 23·43 Å and b = 19·93 Å and composition $Al_{190}Co_{64}$. The 3/4 approximant has not been observed in Al–Co alloys but it provides a bridge between the solved 2/3 Al_3Co approximant and the larger Al–Co approximants reported (Ma and Kuo 1992, 1995, Ma *et al.* 1995), as well as the metastable decagonal phase itself.

The simulation described in § 3 was performed on all three approximants to test the PB–HBS tiling model. Long runs were performed on each approximant and configurations separated by long time intervals were examined from each simulation. A systematic way of associating a PB–HBS tiling with a configuration is needed. Our results suggest that examination of the Co atoms *alone* is sufficient to identify PBs and the puckering pattern. The characteristic of a PB is a Co pentagon at the equator and junction layers with the Co atoms in the puckered layers on pole positions displaced away from the PB equator. We examined the Co positions in each sample configuration to determine the location of PBs. All independent coordinates (x, y) in the site list were considered as possible PB axes. Two PBs, each containing five equator Co atoms and two pole Co atoms, as well as two junction layers each containing five junction Co atoms can be accommodated by the (doubled) c = 16 Å periodicity, for a a total of 24 Co atoms per ideal vertically stacked PBs. For each configuration tested, the number of Co atoms matching Co positions for the ideal PBs was counted for each possible cluster center, and then the centres were ranked in order of agreement with the ideal PB.

Suppose that the simulation of a 3/4 approximant yielded a perfect PB–HBS tiling. There would be a 24-atom (or 100%) coincidence between ideal and actual Co positions for each of the ten PB axes. Additionally, there would be axes external to the actual PB axes with a large coincidence between actual and ideal Co positions. Detailed consideration of the geometry of each possible tiling (fig. 6) shows that the maximum coincidence for an external axis is 16 Co atoms (two thirds of the maximum 24) and that there are several such axes for each tiling. Now suppose, on the other hand, that the simulation structure were completely random. Then the ranked Co coincidence count would be a smoothly decreasing function of rank. The intermediate case of a PB–HBS tiling with slight Co disorder would yield ten axes with nearly perfect agreement and several with close to two-thirds agreement.

The results for our simulation are shown in fig. 7, where we plot the average Co coincidence fraction against rank for the 3/4 approximant simulation. The signature of a PB–HBS tiling with only slight Co disorder is evident. First, the coincidence fraction for ranks 1–10 is close to unity showing that ten PB axes can be identified per configuration. Second, the coincidence fraction jumps discontinuously at rank 11 to a group of axes with close to two-thirds coincidence fraction, suggesting that the

Fig. 6

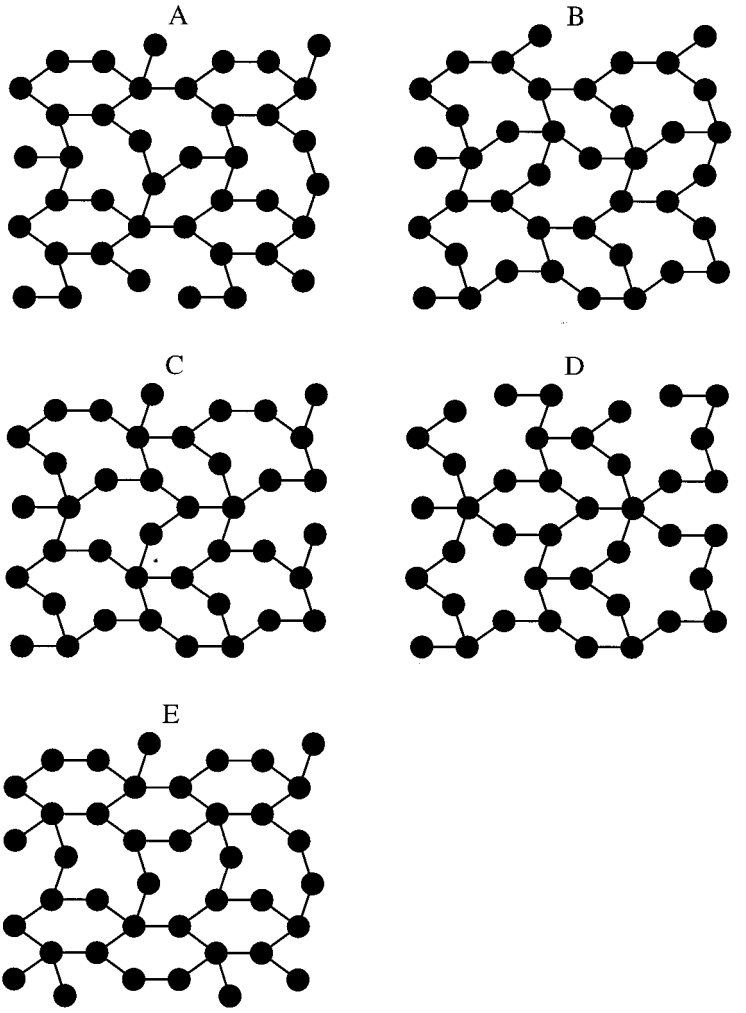

All symmetry-independent HBS tilings allowed for the 3/4 orthorhombic cell.

local environment of the PBs is correct for a PB–HBS tiling. Inspection of representative configurations confirms that the projected PB axes formed a PB–HBS tiling in each case. Finally, for most PB axes, with few exceptions, one centring position (+/-) reproduced the positions of the pole Co atoms significantly better than the other, showing that puckering patterns are also well defined.

The agreement between observed Co positions and those for a perfect PB–HBS tiling is not always exact, as shown by the less than perfect coincidences in fig. 7. Still, for the 3/4 approximant, an average of 97% of the Co atom positions agreed exactly with those of the corresponding perfect PB–HBS tiling. Similar agreement is found for the other approximants studied. We conclude that under pair potentials the PB–HBS tiling model, with the PB puckering Ising variable, is valid for small approximants.

Fig. 7

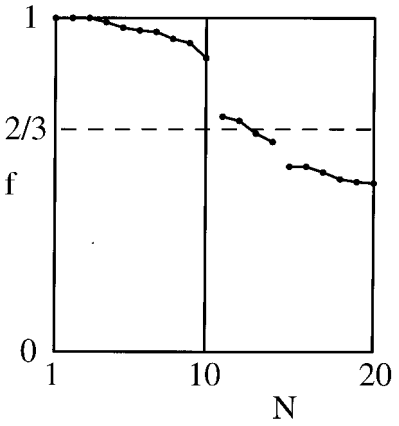

Average coincidence fraction f between Co positions for Nth-best cluster axis in a T = 1000 K Al–Co simulation and the Co positions for perfect PB cluster centred on this axis. The horizontal line at f = $\frac{2}{3}$ represents the maximum coincidence for an axis external to a given PB in a PB–HBS tiling. Note the clear division between PB axes for N ⩽ 10 and non-PB axes for N > 10 as expected in the HBS tiling model.

In both the 2/3 and the 3/2 approximants there is only one possible HBS tiling consistent with the lattice constants, namely the tilings consisting of hexagons only shown in fig. 4. The simulation easily finds (and remains 'locked' on) these tilings, which are the experimentally observed tilings. For the 3/4 approximant, there are five symmetry-independent HBS tilings (see fig. 6). Four of these (B, C, D and E) have mirror or glide planes consistent with full orthorhombic symmetry, while tiling A has only monoclinic symmetry. Three of the five distinct tilings of fig. 6 (B, C and D) were observed in our simulation. With the atomic surface oversizing parameter ϵ that we chose, we lack proper sites to place a complete PB on each vertex of tiling E and did not observe this tiling in our simulation. We suspect that tiling A would appear in a sufficiently long simulation.

A representative atomic structure corresponding to tiling B is shown in fig. 8. The broken lines in fig. 8 indicate the tiling change needed to transform the tiling of type B into type C. The broken lines in fig. 8(*b*) form boundaries of bowtie-shaped regions; thus this flip is called a 'bowtie flip' (Steurer *et al.* 1993, Widom and Cockayne 1995). Each tiling in fig. 6 (and its mirror images) can be reached from the others via a series of bowtie flips.

By inspection of fig. 8, we find a simple description of the atomic motion involved in the bowtie flip. It involves the exchange of an Al–Co pair separated by 2·47 Å in each puckered layer, the exchange of a Co atom with a vacancy or Al atom 5·5 Å away in each flat layer, together with some additional small Al atom phason hops. Details of the flat-layer exchange and Al atom phason hops depend on the local Al configuration.

Individual structures in our 1000 K simulations are not fully stable under relaxation using our pair potentials. We believe this reflects two deficiencies in our modelling effort. First, the ideal sites do not exactly match known positions in small approximants. The atomic surfaces should not be perfectly flat. The median

Fig. 8

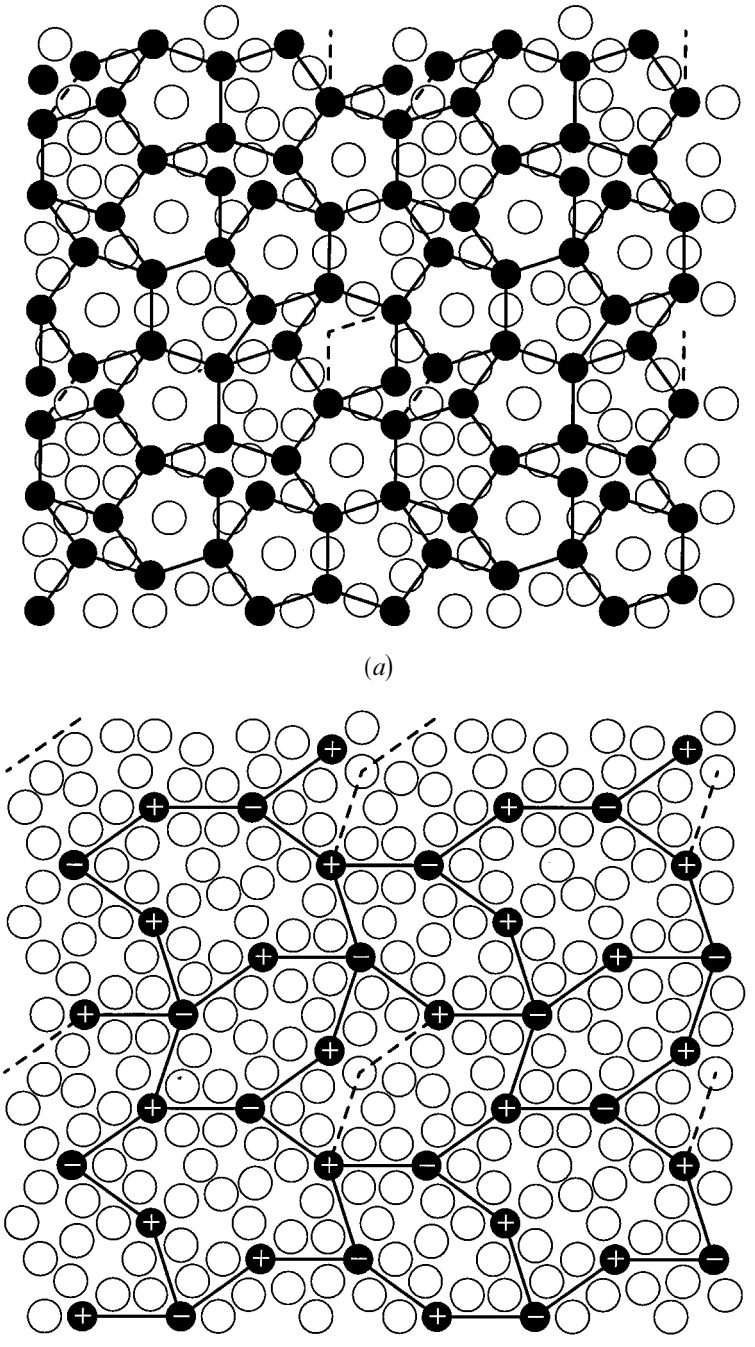

(*a*)

(*b*)

Atomic positions in (*a*) a flat layer and (*b*) a puckered layer for a representative 1000 K simulation configuration. A 2 by 2 supercell of the simulation cell is shown. Open circles denote the Al atoms, while full circles denote the Co atoms. This configuration represents tiling B of fig. 6. The broken lines indicate the single bowtie phason flip per unit cell needed to convert this tiling into a tiling of type C.

displacement under relaxation of 0·2 Å is fairly consistent with the median 0·12 Å deviations of our model from experiment discussed in § 2. Secondly, the pair potentials only approximate the total energy, which should include three- and higher-body interactions. While we believe this has only a small impact on our calculated total energies and the resulting simulated equilibrium ensemble, it can have a considerable impact on relaxation to lowest-energy configurations. There are many nearly degenerate structures differing only by small atomic displacements. Any barrier between such configurations would be small. The lack of many-body interactions then could mean the difference between existence or absence of a barrier in our calculated energy landscape. Where barriers are missing, large displacements may result even though energy changes are small.

Interestingly, in the orthorhombic Al_3Co structure (Grin *et al.* 1994), the largest Debye–Waller factors are reported for those sites in the Al(7)–Al(26) family near the edges of flat-layer pentagons, and their averaged counterparts. These are the atoms that appear most mobile in our simulation. We speculate that the large Debye–Waller factors confirm the very flat energy landscape described above, and these atoms will easily displace under relaxation. A minority (about 2%) of the atoms exhibit relaxations over 1 Å. Most of these large displacements are the central PB Al atom 'off centring'. Whether this is an artefact of the pair potentials or represents an actual displacive transition that takes place at low temperatures is an open question.

Since the experimental evidence suggests that most atoms do indeed sit near our ideal sites, we believe that our discretization of space partially compensates for our lack of many-body interactions. We believe our simulated configurations are closer to experiment than would be possible in the continuum.

PB equators occupied by just one central Al atom are easily distinguished from PB junction layers occupied by up to five Al atoms. The decoration of these flat layers is strongly correlated with the vertical displacement of the Co atoms in adjoining layers. During the simulation the flat-layer Al decoration fluctuates in tandem with the 'puckering' discussed in the introduction. There is greater variability in the flat-layer Al configuration than may be accounted for by the puckering fluctuations alone. The PB junction layers, in particular, do not exhibit a unique Al pattern. The Al concentration is sufficiently low that plenty of energetically reasonable atomic sites remain empty. Many more sites remain that cannot be occupied owing to overlap with a nearby Al atom but can become occupied once the nearby Al atom moves elsewhere. As the simulation progresses, a vast number of distinct Al configurations are visited that are all compatible with a given PB tiling and puckering pattern.

Table 2 gives the simulation average electron count per unit cell due to each atomic surface type, based on results for the 3/4 approximant at 1000 K. The 'dominant' atomic surfaces (based on average electron count times multiplicity) for the flat layers are, in order, the $\upsilon = 0$ atomic surface associated with the network of Co pentagons, the $\upsilon = 2, 3$ atomic surfaces associated with the PB junction layer Al atoms, the 'averaged' atomic surfaces associated with Al atoms on the edge of a Co pentagon, and the $\upsilon = 1, 4$ atomic surfaces associated with the PB centre Al atoms. The dominant atomic surfaces for the puckered layers are the $\upsilon = 1, 4$ atomic surfaces containing all the PB cap atoms and the 'averaged' atomic surfaces for unpuckered atoms near the centres of the tiles. It is interesting to note that the puckered-layer level 0, 2 and 3 atomic surfaces had strictly zero occupancy in the simulations. This implies that there is little tendency for reconstruction in this approximant.

Fig. 9

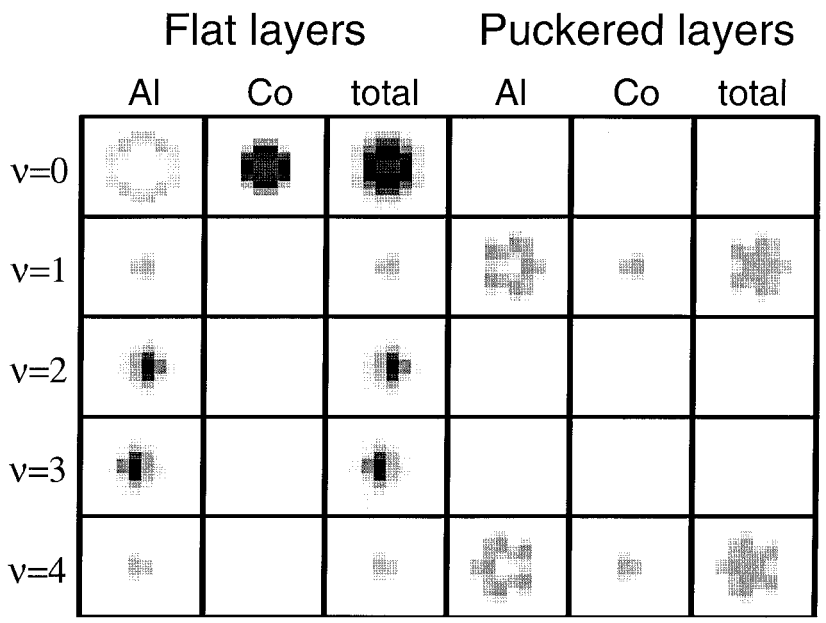

Maps of the atomic surfaces obtained by simulating an Al–Co 3/4 orthorhombic approximant at T = 1000 K.

The *average* structure obtained can be conveniently displayed as atomic surface maps. Figure 9 shows maps of mean Al, Co and total occupancy of each integer coordinate atomic surface that is occupied during the 1000 K 3/4 simulation. The discreteness of the maps is due to the finite approximate size. The pseudopentagonal symmetry of the individual atomic surfaces is clear, particularly for the $\upsilon = 1$ and 4 puckered-layer atomic surfaces. The flat-layer atomic surfaces at $\upsilon = 0$, and puckered-layer atomic surfaces at $\upsilon = 1$ and 4 consist of cores that are primarily Co, and Al on the outsides, while the other atomic surfaces are nearly entirely occupied by Al. The occupancy probability of the flat-layer $\upsilon = 2$ and 3 atomic surfaces fall off rather smoothly near the atomic surface edges. Partial occupancy is the crudest characterization of disorder. We have also investigated pair correlation functions, defined by subtracting the product of two individual site occupancies from the probability of simultaneous occupation of those two sites. The strongest correlations found are negative correlations between sites separated by less than 2 Å and are due to the short-range interatomic repulsion.

Partial Al occupancy corresponds mainly to variability in the junction layer decoration described above. Coordinated phason fluctuations that rearrange the HBS tiling, in contrast, require both Al movements and Al–Co exchange. This causes the partial Al occupancy near the edges of the puckered-layer atomic surfaces, as well as a thin zone of mixed Al–Co occupancy separating the Co and Al zones in the mixed atomic surfaces. In physical space, a Co–Al pair separated by 2·47 Å exchanges in each puckered layer, while a Co atom in the junction layer exchanges with an Al or vacancy 5·5 Å away (see broken lines in fig. 8).

Finally, we discuss the disorder in the Co atom positions. On average, 3% of Co atoms are not on ideal PB–HBS tiling positions at T = 1000 K. We systematically

investigated these defects and found that nearly all of them (95%) involve the type of Co motion associated with a phason flip (2·47 Å horizontal in a puckered layer or 5·5 Å horizontal in a flat layer) or a puckering flip (0·52 Å vertical motion of the pole atom). These defects create stacking disorder because they occur in some, but not all, atomic layers. About a third of such defects displace Co atoms to a new position that is incompatible with a PB tiling; however, these defects were always isolated, while the Co defects compatible with the bowtie flip mentioned above often occur in a coordinated way in several layers to change the tiling. Incidentally, in the high-temperature 4 Å $Al_{11}Co_4$ phase, the Al and Co positions are interchanged with respect to the PB cap decoration, that is the 2·47 Å horizontal Al–Co exchange actually becomes favoured in free energy.

That observation reveals the chemical nature of phason hops in this system, and in chemically ordered systems in general. Exchanges used in our simulation are long-range with unphysical dynamics, but correct equilibrium properties. We conclude that the energy difference between a perfect PB–HBS tiling and one with bowtie flips in some layers is much less than the energy barrier associated with the Co atom in an intermediate position (which was not observed in the sampled configurations). Chemical ordering is a problem for phason dynamics, because the short (less than 2 Å) atomic phason hops in realistic atomic models destroys the chemical ordering. Preserving chemical order in the PB–HBS tiling model requires Co motion greater than 2 Å. Our simulations suggest a hierarchy of phason motion; short (less than 2 Å) mainly Al atom phason hops, and correlated phason flips that transport Co atoms more than 2 Å to their positions in another chemically ordered structure. The Co atoms spend a statistically insignificant time at intermediate positions. Examination of the physically plausible local swaps and hops suggests that mobility of Co atoms increases greatly when some nearby Al sites are vacant. Our observations on Co hopping are consistent with the kinds of vacancy-assisted hopping and diffusion discussed by Coddens *et al.* (1993) and Zumkley *et al.* (1996).

4.2. *Energetics*

We examine the energetics of single-atom displacements and multiple-atom 'flips' associated with distinct tilings and distinct patterns of puckering. At a temperature of 1000 K we observe fast fluctuations of certain Al sites in addition to slow evolution of the Co positions. To investigate the nature of the excitations in more detail, we first cooled the 3/4 approximant to absolute zero temperature via simulated annealing; then we ran the Monte Carlo simulation discussed in § 3, still at absolute zero. Our annealed configuration is metastable because no hops or swaps are successful at 0 K. Energy increases of the *attempted* motions are the energies of the low-lying one- and two-atom excitations. Figure 10 shows the frequency of attempted processes as a function of energy change for those Al hops, Co hops and Al–Co swaps of less than 2·5 Å and $\Delta E < 2$ eV which are most likely to be physical. The corresponding hops or swaps are identified in table 3.

Two spectral features worth noting. Firstly the spectra for Al and Co hops contain sharp peaks at low energies and show no overall increase between 0 and 2 eV. The spectrum for Al–Co swaps, on the other hand, rises as a broad continuum as the energy increases. Secondly there are many more distinct low-energy Al hops than low-energy Co hops. The only low-energy Co hops observed that contain a phason component are 2·34 and 2·47 Å hops to nearby empty sites. Interestingly, both of these hops involve the kind of junction layer site indicated by an × in fig.

Fig. 10

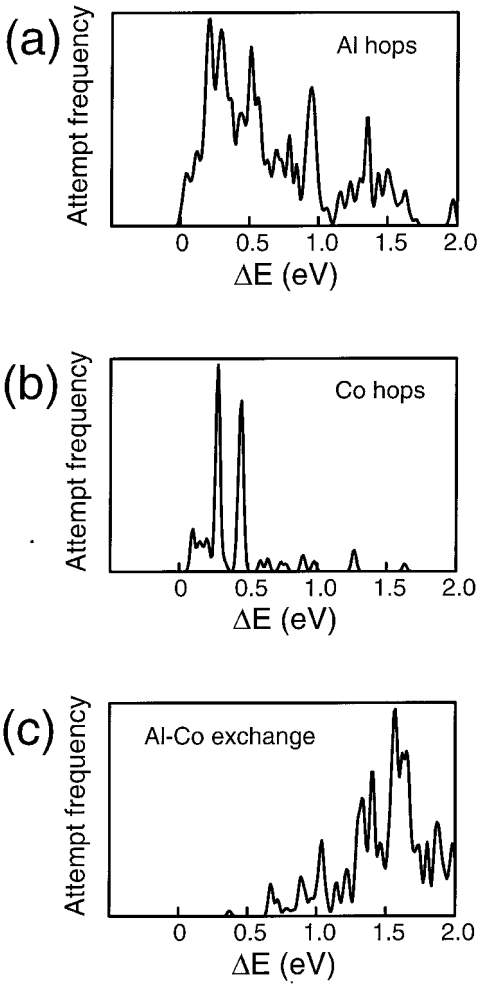

'Energy spectra' for (*a*) short Al hops, (*b*) short Co hops and (*c*) short Al–Co swaps.

Table 3. Prominent low-energy peaks in excitation spectra (figs. 10(*a*) and (*b*)) and associated atomic motion.

Energy (eV)	Move type
0·04	Al 0·765 Å
0·10	Co 2·339 Å
0·12	Al 0·520, 0·539 Å
0·15	Co 2·339 Å
0·20	Co 0·520 Å
0·21	Al 0·539 Å
0·28	Co 0·260 Å
0·29	Al 0·520 Å
0·45	Co 0·260 Å
0·51	Al 0·520, 0·945 Å

2(*c*). In fact, during the simulated annealing, three out of 128 Co atoms moved off puckered-layer PB pole positions via 2·34 Å hops to these vacant junction layer sites. The lowest-energy Co phason excitations simply move those Co atoms back to the PB poles. Curiously, there are more Co atoms on ideal PB positions on average at 1000 K than at 0 K. The slower rate for Co motion may be due to the need for Al vacancy assistance, rather than the relatively strong binding of Co compared with Al.

It would be useful to establish an effective free energy for different tilings and puckering patterns, in which the Co atoms are frozen in the PB–HBS tiling positions and the fast Al fluctuations are 'integrated out'. Formally, the full partition function can be written

$$Z = \sum_{\{\text{Co positions}\}} \sum_{\{\text{Al positions}\}} \exp\left(-\frac{E}{k_B T}\right) = \sum_{\{\text{Co positions}\}} \exp\left(-\frac{F_{\text{eff}}}{k_B T}\right), \qquad (7)$$

and the effective free energy may be decomposed into

$$F_{\text{eff}} = U_{\text{eff}} - TS_{\text{eff}}. \qquad (8)$$

Determination of F_{eff} would replace the complex problem of atomic-level thermodynamics with a simpler tiling model thermodynamics containing terms for individual tile energies and entropies as a function of temperature and corrections for the energy and entropy interactions between tiles.

The inner sum in eqn. (7) can be evaluated, up to an overall constant factor, by simulating the Al motion while holding the Co atoms fixed. The energy component U_{eff} is the average of the instantaneous total energies. The entropy S_{eff} may not be so easily evaluated. For the present we consider the partial information provided by the energy alone. We investigated the dependence of U_{eff} on the PB tiling and puckering pattern. Our results show small, but measurable, effects of tiling and puckering patterns on energy. The energy differences among tilings with the same numbers of hexagons, boats and stars are typically in the range of 0·001 eV atom^{-1}. There is a larger energy change, about 0·002 eV atom^{-1}, for replacing a pair of boats with a star and a hexagon. Quantitative data for some of the structures simulated is presented in table 4.

During a run the internal energy constantly fluctuates. From the calculated heat capacity (about 0·3k_B atom^{-1}) at T = 1000 K, with 508 atoms we find rms deviations of total energy of 1·1 eV, or 0·002 eV atom^{-1}. This energy scale for single-atom fluctuations is slightly larger than the energy differences between distinct tilings. That explains why the system evolves among distinct tilings during the simulation.

Table 4. Selected results for simulations with fixed Co patterns. Data based on three runs of 150000 attempted Monte Carlo steps per atom for each tiling and spin configuration. The form of a two-interaction tiling Hamiltonian for U_{eff} is also shown.

Type	U_{eff}	Energy (eV atom^{-1})	Specific heat (units of k_B)
B antiferromagnetic	$U_B - 14J + 10K$	0·113 37(7)	0·280(9)
B ferromagnetic	$U_B + 14J + 10J$	0·112 75(5)	0·275(7)
C antiferromagnetic	$U_C - 14J + 10K$	0·113 85(6)	0·299(7)
C ferromagnetic	$U_C + 14J + 10K$	0·113 31(4)	0·293(5)
D antiferromagnetic	$U_D - 14J + 11K$	0·116 02(4)	0·285(8)
D ferromagnetic	$U_D + 14J + 11K$	0·114 67(7)	0·288(6)

It also means that the effective energy U_{eff} is sensitive to each atomic position, and therefore sensitive to the presence or absence of individual sites in our ideal site list. The details of the site list may dominate differences in effective energies between configurations, with the true energy differences between tilings being immeasurably small by our method.

We attempted to describe the puckering energetics in terms of the Ising spin model described in the Introduction. For each PB (labelled *i*) we define the Ising spin s_i. The effective energy is a function of the tiling and the spin configuration because these, together, define the Co positions. Since the puckering patterns of experimental Al_3Co and $Al_{13}Co_4$ are neither 'ferromagnetic' nor 'antiferromagnetic' (see fig. 4), we include second-nearest-neighbour terms. It is plausible that first- and second-neighbour terms dominate the puckering energetics because, in these cases, two PBs share atoms. In the hope that the Ising variables decouple from the tiling we write the effective Hamiltonian

$$U_{\text{eff}} = U_{\text{eff}}(\text{tiling}) + \sum_{1\text{nn}} J s_i s_j + \sum_{2\text{nn}} K s_i s_j. \tag{9}$$

To determine the magnitudes of J and K, we produced a series of different puckering configurations for the tilings. For each basic tiling, we chose fully antiferromagnetic and ferromagnetic puckering patterns (see table 4) to give the greatest possible range in J at fixed positive K, other patterns that maximize the negative contribution of K, and random patterns. The average internal energy differences among patterns are typically of the order of 10^{-4} eV atom^{-1}, implying values of J and K of the order of 10^{-5} eV atom^{-1}. These energy differences are small compared with energy fluctuations for single-atom displacements.

If the two-coupling model of eqn. (9) were a good approximation, then the internal energies of all puckering patterns investigated for each tiling could be fitted with little error. Unfortunately, it is not a good approximation, as the rms error of the two-coupling model fit is 5×10^{-4} eV atom^{-1}, which is the same order of magnitude as the differences in energy of the puckering patterns being fitted. We believe that this failure reflects both a true failure of such a simple model and a systematic difficulty with our approach. To illustrate the first point, consider the junction layers, and let all the junction layer Al atoms either form distorted pentagons as shown in fig. 2 or sit on subsets of this pentagon. A full description of a configuration must specify the orientation of this distorted pentagon, that is, the direction of the junction layer arrow shown in fig. 2. Preferred orientations are coupled with the Ising puckering variable and the local tiling. Even if an accurate tiling Hamiltonian with short-range pairwise interactions exists for the combination of puckering and arrow variables, averaging over arrow orientations as in eqn. (7) will probably generate long-range and multiple spin effective Ising interactions. We conclude that longer-range and/or many-cluster effects are important for stabilizing certain puckering patterns in Al_3Co. In our approach, the issue is further complicated because we did not base our site list on considerations of junction layer pentagon orientation and do not even have the necessary sites to allow all orientations for each junction layer.

§ 5. Conclusions

We reach several conclusions as a result of our study. This section summarizes real and perpendicular space descriptions of 8 Å Al–Co structure and fluctuations, together with a description of possible improvements and directions for future work.

Our simulations reveal strong preference for spatial arrangements of atoms that fill space with PB clusters. These arrangements place clusters at vertices of some HBS tiling with edge length 6·5 Å. We have previously shown that the oscillating form of the pair potentials favours PB clusters because pair potential minima match important characteristic distances within each PB and linking neighbouring PBs (Widom and Cockayne 1996). At a simulation temperature of 1000 K, there is some disorder in Co atom location, but each Co pattern observed in a simulation on a 24 Å by 20 Å by 16 Å approximant can be associated uniquely with a HBS tiling. With each tiling there is associated a 'puckering pattern' according to which flat layer each cluster is centred on. Different tilings occur during the 1000 K simulation, as well as different puckering patterns for each individual tiling. While the puckered-layer Al positions are generally well defined, many different Al arrangements are observed in the flat layers at 1000 K. Puckering disorder at the temperature where the quasicrystal is metastable is likely to lead to an average structure with 4 Å periodicity and P10/mmm symmetry.

We have determined the Co positions and the Al occupancies in the hexagon, boat and star tiles in our approximants. The hexagon, boat and star tiles are sufficient for generating quasiperiodic structures and a simple extension of our results leads to atomic models for such quasicrystals. The bowtie phason flips that change the tiling in our simulations on approximants should also occur in the quasicrystal.

Atomic sites in our model quasicrystal are intersections of atomic surfaces with physical space. To model all the sites in the observed Al_3Co approximants requires a few small atomic surfaces whose 5D coordinates include half-integers as well as several large atomic surfaces associated with integer coordinates. as listed in table 2. Because we choose over-sized atomic surfaces, we do not need to know or presuppose detailed atomic surface shapes. Indeed, we find that a statistical description of atomic surfaces is necessary at a temperature of 1000 K. When both Al and Co share an atomic surface, the Co occupies the middle, while the Al forms a shell around it. There is a smooth fall-off in occupation probability near the boundaries of the surfaces and a smooth transition of occupation probability from Co to Al. Both these smooth transitions reflect distinct forms of phason disorder.

Our simulation visits an entire family of probable configurations. This includes both ideal cluster packings and characteristic low-energy fluctuations that transform one ideal structure into another. By far the most common type of fluctuation is movement of those Al atoms near the atomic surface edges. The Co positions change with much lower frequency. We believe that the Co mobility is highly dependent on the presence of Al vacancies. From the attempted hop energy spectra in fig. 10 we note that many possible hops require less than $5k_BT$ (= 0·43 eV at T = 1000 K) energy, implying a reasonable chance for acceptance. Indeed, there is no effective lower bound on the attempted hop energy. Our simulation continues to display Al vacancy hopping at room temperature (T = 300 K) and below. Because these atoms occupy sites near the atomic surface edges, the vacancy hopping is a type of phason fluctuation.

Al motion and Al–Co swaps contribute to two kinds of collective fluctuation in our simulations that preserve the PB–HBS description. One of these (the 'puckering flip') shifts a column of clusters 4 Å along its axis; the other (the 'phason flip') moves a column of clusters 2·5 Å in a direction perpendicular to its axis and rotates it 180°. In each flip, most atoms remain stationary or move very small distances. Puckering flips occur with greater frequency than phason flips. Our observation of puckering

reversals within a given tiling, and phason flips between tilings, implies that the energy cost of such fluctuations is low enough that they occur readily in equilibrium at T = 1000 K.

We now summarize possible inadequacies of our methods and results. The ideal sites do not capture the observed Al and Co positions exactly. While the median distance of experimental sites from ideal is 0·12 Å, a few sites lie as much as 0·58 Å away. Furthermore, a small number of atoms exhibit large displacements under relaxation from their ideal positions. We believe that present Al–TM pair potentials are inadequate to treat relaxation properly.

The comparative energetics of differing tilings and puckering patterns are very sensitive to the inclusion or exclusion of certain sites, in particular the special sites in the flat and puckered layers. To make matters worse, our site list constructed according to the discussions of § 2 does not yield full local fivefold rotational symmetry within PB clusters, introducing the systematic error discussed in the previous section. To investigate sensitivity to the site list, we added carefully chosen sites to the site list, especially those that maximize local pentagonal symmetry on possible cluster axes. Simulations confirmed that the energy depends on inclusion of particular sites at a level comparable with the energy differences between distinct tilings. Our results for the energy differences between tilings must thus be taken as upper estimates only.

We have not found a temperature-dependent effective tiling Hamiltonian. Such a Hamiltonian, once obtained, would allow simulation studies of the fundamental and interesting question of the nature of the stability of the quasicrystalline phase. Further progress requires both a new method for site list construction that respects local symmetry, and inclusion of long-range and many-body couplings in the effective Hamiltonian.

Finally, we compare this work with similar efforts. Mihalkovič *et al.* (1996a,b) used pair potentials to find tile energies and interaction energies of tiles for a canonical cell model of i-(Al–Mn) at zero temperature and succeeded in creating a 'zero-temperature' tiling Hamiltonian. We focused, on the other hand, on finite-temperature structures and found a large source of entropy due to Al rearrangements within the tiles that we were unable to quantify. Based on the large number of Al sites with partial occupancy, and the small number of different tilings, the internal Al disorder entropy is likely to be larger than the tiling entropy at 1000 K (for a tiling description on the 6·5 Å length scale). We conjecture that this is true for complex Al–TM phases in general.

Dmitrienko and Astraf'ev (1995) combined energetics with a growth model to define a set of ideal sites. That is, their site list evolved as the quasicrystalline structure grew. An approach of this type might help to solve our problem of systematic errors in U_{eff} arising from the site list construction. The idea would be to replace the site list with atomic surface occupancy directly in the higher-dimensional space. The equivalent of our discretization of space would be placing a limit on perpendicular space deviations between neighbouring atoms. The fall-off in atomic surface occupancy near the edges suggests such a cut-off may easily be implemented.

ACKNOWLEDGEMENTS

We wish to acknowledge useful discussions and assistance from J. Zou, R. Phillips, A. E. Carlsson, C. L. Henley and R. H. Swendsen. We also thank C. L. Henley for his comments on the manuscript. This work was supported in part under National Science Foundation grant No. DMR-9221596.

References

Bak, P., 1986a, *Phys. Rev. Lett.*, **56**, 861; 1986b, *Scripta metall.*, **20**, 1199.

Beeli, C., and Horiuchi, S., 1994, *Phil. Mag.* B, **70**, 215.

Burkov, S. E., 1991a, *J. statist. Phys.*, **65**, 395; 1991b, *Phys. Rev. Lett.*, **67**, 614.

Cockayne, E., 1995, *Phys. Rev.* B, **51**, 14 958.

Cockayne, E., Phillips, R., Kan, X. B., Moss, S. C., Robertson, J. L., Ishimasa, T., and Mori, M., 1993, *J. non-crystalline Solids*, **153–154**, 140.

Coddens, G., Soustelle, C., Bellissent, R., and Calvayrac, Y., 1993, *Europhys. Lett.*, **23**, 33.

Dmitrienko, V. E., and Astaf'ev, S. B., 1995, *Phys. Rev. Lett.*, **75**, 1538.

Edagawa, K., Suzuki, K., Ichihara, M., and Takeuchi, S., 1991, *Phil. Mag.* B, **64**, 629.

Fettweis, M., Launois, P., Dénoyer, F., Reich, R., and Lambert, M., 1994, *Phys. Rev.* B, **49**, 15 573.

Frenkel, D. M., Henley, C. L., and Siggia, E. D., 1986, *Phys. Rev.* B, **34**, 3649.

Gähler, F., 1988, PhD Thesis, Swiss Federal Institute of Technology, Zürich.

Grin, J., Burkhardt, U., Ellner, M., and Peters, K., 1994, *J. Alloys Compounds*, **206**, 243.

Grushko, B., Wittenberg, R., Bickmann, K., and Freiburg, C., 1995, *Proceedings of the Fifth International Conference on Quasicrystals*, edited by C. Janot and R. Mosseri (Singapore: World Scientific), p. 684.

Henley, C. L., 1991, *Quasicrystals: The State of the Art*, edited by D. P. DiVincenzo and P. J. Steinhardt (Singapore: World Scientific), p. 429; 1993 *J. non-crystalline Solids*, **153–154**, 172.

Hiraga, K., Lincoln, F. J., and Sun, W., 1991, *Mater. Trans. Japan Inst. Metals*, **32**, 308.

Hudd, R. C., and Taylor, W. H., 1962, *Acta crystallogr.*, **15**, 441.

Ingersent, K., 1991, *Quasicrystals: the State of the Art*, edited by D. P. DiVincenzo and P. J. Steinhardt (Singapore: World Scientific), p. 185.

Jeong, W.-C., and Steinhardt, P. J., 1993, *Phys. Rev.* B, **48**, 9394.

Krajčí, J., Hafner, J., and Mihalkovič, M., 1997, *Phys. Rev.* B, **55**, 843.

Li, X. Z., 1995, *Acta crystallogr.* B, **51**, 265.

Li, X. Z., and Dubois, J. M., 1994, *J. Phys: condens. Matter*, **6**, 1653.

Li, X. Z., and Kuo, K. H., 1991, *Proceedings of the China Japan Seminars*, edited by K. H. Kuo and T. Ninomiya (Singapore: World Scientific), p. 102.

Li, X. Z., Ma, X. L., and Kuo, K. H., 1994, *Phil. Mag. Lett.*, **70**, 221.

Li, X. Z., Shi, N. C., Ma, L. S., Ma, X. L., and Kuo, K. H., 1995, *Phil. Mag. Lett.*, **72**, 79.

Liao, X. Z., Kuo, K. H., Zhang, H., and Urban, K., 1992, *Phil. Mag.* B, **66**, 549.

Lubensky, T., 1988, *Introduction to Quasicrystals*, edited by M. V. Jarič (New York: Academic Press), p. 199.

Ma, X. L., and Kuo, K. H., 1992, *Metall. Trans.* A, **23**, 1121; 1995, *Phil. Mag.* A, **71**, 687.

Ma, X. L., Li, X. Z., and Kuo, K. H., 1995, *Acta crystallogr.* B, **51**, 36.

Mahne, S., and Steurer, W., 1996, *Z. f Kristallogr.*, **211**, 17.

Metropolis, N., Rosenbluth, A. W., Rosenbluth, M. N., Teller, A. H., and Teller, E., 1953, *J. chem. Phys.*, **21**, 1087.

Mihalkovič, M., Zhu, W.-J., Henley, C. L., and Oxborrow, M., 1996a, *Phys. Rev.* B, **53**, 9002.

Mihalkovič, M., Zhu, W.-J., Henley, C. L., and Phillips, R., 1996b, *Phys. Rev.* B, **53**, 9021.

Niizeki, K., 1994, *Mater. Sci. Forum*, **150–151**, 155.

Olamy, M., and Kléman, M., 1989, *J. Phys., Paris*, **50**, 19.

Phillips, R., and Widom, M., 1993, *J. non-crystalline Solids*, **153–154**, 416.

Phillips, R., Zou, J., Carlsson, A. E., and Widom, M., 1994, *Phys. Rev.* B, **49**, 9322.

Shin, M., and Strandburg, K. J., 1993, *J. non-crystalline Solids*, **153–154**, 253.

Socolar, J. E. S., 1991, *Quasicrystals: the State of the Art*, edited by D. P. DiVincenzo and P. J. Steinhardt (Singapore: World Scientific), p. 213.

Steurer, W., 1991, *J. Phys.: condens. Matter*, **3**, 3397.

Steurer, W., Haibach, T., Zhang, B., Beeli, C., and Nissen, H.-U., 1994, *J. Phys.: condens. Matter*, **6**, 613.

STEURER, W., HAIBACH, T,., ZHANG, B., KEK, S., and LÜCK, R., 1993, *Acta crystallogr.* B, **49**, 661.
STEURER, W., and KUO, K. H., 1990, *Acta crystallogr.* B, **46**, 703.
STOUT, G. H., and HENSEN, L. H., 1989, *X-ray Structure Determination: A Practical Guide* (New York: Wiley), p. 370.
STRANDBURG, K., TANG, L. H., and JARIČ, M. V., 1989, *Phys. Rev. Lett.*, **63**, 314.
TANG, L. H., 1990, *Phys. Rev. Lett.*, **64**, 2390.
TANG, L. H., and JARIČ, M. V., 1990, *Phys. Rev.* B, **41**, 4524.
TSAI, A. P., INOUE, A., and MASUMOTO, T., 1987, *Jap. J. appl. Phys.*, **2**, L1505; 1989, *Mater. Trans. Japan Inst. Metals*, **30**, 463.
TSAI, A. P., INOUE, A. YOKOYAMA, Y., and MASUMOTO, T., 1990, *Mater. Trans. Japan Inst. Metals*, **31**, 98.
WIDOM, M., 1990, *Quasicrystals*, edited by M. V. Jarič and S. Lundqvist (Singapore: World Scientific), p. 337.
WIDOM, M., and COCKAYNE, E., 1995, *Proceedings of the Fifth International Conference on Quasicrystals*, edited by C. Janot and R. Mosseri (Singapore: World Scientific), p. 343; 1996, *Physica* A, **232**, 713.
WIDOM, M., DENG, D. P., and HENLEY, C. L., 1989, *Phys. Rev. Lett.*, **63**, 310.
WIDOM, M., PHILLIPS, R., ZOU, J., and CARLSSON, A. E., 1995, *Phil. Mag.* B, **71**, 397.
YAMAMOTO, A., KATO, K., SHIBUYA, T., and TAKEUCHI, S., 1990, *Phys. Rev. Lett.*, **65**, 1603.
ZOU, J., and CARLSSON, A. E., 1993a, *Phys. Rev. Lett.*, **70**, 3748; 1993b, *Phys. Rev.* B, **47**, 2961.
ZUMKLEY, TH., MEHRER, H., FREITAG, K., WOLLGARTEN, M., TAMURA, N., and URBAN, K., 1996, *Phys. Rev.* B, **54**, R6815.